2021-01-0647 Published 06 Apr 2021

Effect of Swirl Ratio and Piston Geometry on the Late-Compression Mean Air-Flow in a Diesel Engine

Ashutosh Jena, Harsimran Singh, and Avinash Kumar Agarwal Indian Institute of Technology Kanpur

Citation: Jena, A., Singh, H., and Agarwal, A.K., "Effect of Swirl Ratio and Piston Geometry on the Late-Compression Mean Air-Flow in a Diesel Engine," SAE Technical Paper 2021-01-0647, 2021, doi:10.4271/2021-01-0647.

Abstract

The rising concerns of emissions have put enormous strain on the automotive industry. Industry is, therefore looking for next-generation engines and advanced combustion technologies with ultra-low emissions and high efficiency. To achieve this, more insights into the combustion and pollutant formation processes in IC engines is required. Since conventional measures have not been insightful, in-situ measurement of combustion and pollution formation through optical diagnostics is being explored. Gaining full optical access into the diesel engine combustion chamber is a challenging task. The late-compression flow dynamics is not well understood due to limited access into the engine combustion chamber. These flow structures contribute immensely to fuel-air mixing and combustion. The objective of this study is to understand the role of combustion chamber design on vertical plane air-flow structures. A realistic bowl geometry was modeled and simulated using CONVERGE under non-firing conditions to study the flow dynamics. These results were validated with the flow-field of a light-duty optical engine, obtained through Time-Resolved Particle Image Velocimetry (TR-PIV). Further, simulations were carried out using two different bowl geometries. The effect of variations in geometry on turbulent kinetic energy (TKE) was investigated.

Introduction

Implementation of strict emission norms globally and continued pursuit for efficient engines is motivating scientists to develop advanced IC engine technologies. In foreseeable future, the heavy vehicle industry would continue to rely on diesel engines. However, diesel emission remains a serious concern. During diffusion combustion phase in diesel engines, oxidation limit of particulates and unburned fuel is primarily influenced by the mixing rate of fuel and particulate matter (PM) with oxidants. Turbulent flow structures are responsible for proper mixing and late-cycle oxidation reactions [1]. In compression stroke of the engine, turbulence levels are significantly affected by large-scale flow-field [2, 3, 4, 5, 6, 7, 8]. Improved combustion and reduction in emission levels can be achieved with optimization of in-cylinder fuel-air mixing [9]. Strong interactions occur between squish and swirl-flow near the end of the compression stroke. It is believed that squish flow has a dominant effect in disturbing radial distribution of swirl velocity and ideal solid-body like flow structures. By virtue of this, vortices are produced, which generate additional turbulence [2,10]. Understanding of flow during the compression stroke is a pre-requisite for understanding and further optimization of diesel engine performance, optimizing injector location, and minimizing plume-to-plume variations. Late compression flow dynamics is affected by many factors, out of which, most dominant factors are swirl and tumble ratio, piston bowl geometry, squish flow magnitude, and intake port design. Interestingly, higher swirl motion (ideal solid body rotation) does not mean high TKE. Several studies have reported lower turbulence levels with increased swirl ratio [10, 11, 12]. Turbulence level depends upon the production and dissipation rate, given by equation [1] below:

$$\frac{Dk}{Dt} = P - \varepsilon - \left(\nabla . T\right) \tag{1}$$

Thus, it is essential to investigate the physics of fluid-flow dynamics, especially that of late compression flows and their effect on mixture formation and combustion processes. Researchers have found significant improvement in late-cycle mixing by optimizing the piston bowl geometry [13]. Eismark et al. [14] proposed a mechanism to understand radial mixing and investigated the effect of wave-shaped protrusion in the bowl. The radial mixing was found to be superior than conventional design, which resulted in higher rate of soot oxidation. Bianco et al. [15] developed a hybrid piston model by combining stepped-lip geometry and piston with wave protrusion. The study predicted up to 75% soot reduction without compromising the efficiency. Authors also highlighted further scope in CFD optimization for in-cylinder pollutant reduction. Similar reduction in soot was also reported by optimization of Lateral Swirl Combustion Chamber [16]. Piston geometry optimization studies have shown promising results for advanced low-temperature combustion like RCCI and GCI [17, 18]. Despite the proven impact of flow dynamics on engine

performance, investigations of the in-cylinder flow-field have been a challenging task for the majority of researchers because of difficulties associated with optical access into the combustion chamber. Over the past few decades, computational fluid dynamics (CFD) has emerged as an excellent design tool to predict the in-cylinder dynamics. However, the flow and combustion models need continuous inputs from experiments to yield reliable results.

Globally, various studies combining PIV and CFD packages have been done to understand the in-cylinder flow structures and their effects on engine performance. Zha et al. [19] conducted PIV for in-cylinder flows during compression stroke using silica piston with re-entrant bowl geometry. Numerical simulation was also carried out through the CONVERGE CFD package. They concluded that for the range of swirl ratios (2.2 and 3.5), it is the piston geometry that affects late compression mean-flow asymmetry to a greater extent than intake flow methods. Fridriksson et al. [20] investigated the effect of swirl ratio and piston bowl geometry on in-cylinder velocity profile at 30 CAD ATDC. The observations indicated that narrow and deeper piston geometries resulted in an increment in near-wall velocities and reduction in rotational motion in the bowl area since the swirling ratio changed from high to low. This leads to reduction in convective heat loss and an increase in thermal efficiency. Deslandes et al. [21] investigated the effect of piston geometries with flat and bowl-in-piston designs on the swirl center location and turbulent kinetic energy (TKE). They found that bowl-in-piston geometry shows less dispersion in the swirl center position as compared to flat piston. On the other hand, swirl intensity dispersion and TKE slightly increases due to flow transfer from cylinder into bowl. Achuth et al. [22] studied the effect of intake design on tumble flow and concluded that chamber geometry significantly regulates the bulk motion and the turbulence magnitude. Gafoor and Gupta [9] found that the ratio of piston to bowl diameter plays a critical role in swirl ratio optimization. They also highlighted the effect of large swirl ratio and high TKE on the combustion characteristics.

Despite increasing attention in the area of optical diagnostics of flow, the role of combustion chamber geometry is far from understood. This issue is more critical for late compression stages due to limited optical access. Geometric optimization by CFD is promising but comes at the cost of large computational time. Full geometry simulation is capable of capturing local vortices and small-scale structures during induction. However, most of this energy gets dissipated in the late compression phase [23]. Therefore, sector geometry simulation for geometric optimization of diesel engine combustion chamber can be a cheaper alternative. Sector simulation has been widely adopted for prediction of combustion [24, 25, 26]. However, not much work has been done in the area of flow investigations. In this study, sector simulation has been used to study late compression flow dynamics. The effect of geometry and swirl ratio has been investigated. A simplistic bowl and two realistic bowl geometries have been simulated for comparison. Simplistic bowls are common to optical engines. However, the optical access to the vertical plane is often restricted by the bowl rim near TDC. In this study, the vertical plane flow structure has been correlated with the velocity field in the swirl plane. A comparison of the sector simulation vs. full geometry simulation has been done to study the feasibility of this method.

Experimental Setup

The experimental data used for validation were obtained at Sandia National Laboratory using a light-duty optical diesel engine. The optical access was possible via a fused silica window and a realistic geometry optical piston.

The engine can be operated at different swirl ratios by adjusting the throttle openings of tangential and helical ports. Engine details and operating conditions are given intable1. More details of the experimental setup can be found in the original work [27].

Numerical Setup

Simulations were carried out using a commercial CFD solver package CONVERGE [28]. The solver was used to solve Reynolds Average Navier Stokes equation. Turbulence was modeled using Renormalization Group (RNG) closure for the two-equation k-ϵ model. Near-wall velocity field was resolved using the law of wall model. O'Rourke and Amsden heat model was used to simulate the heat transfer. The piston surface geometry for the base model was obtained from the ECN database. The other two geometries, cyl_bowl and erl_bowl were adopted from the Single Cylinder Research Engine (SCRE) at Engine Research Laboratory, IIT Kanpur. Figure 1 shows the geometry of the three different bowls used in this study.

The velocity profile in the engine sector was initialized by using the Bessel function [29]. The velocity profile can be generated by using the equation

$$v(r) = \frac{\omega_c R R_{S0} \alpha}{4 J_2(\alpha)} J_1\left(\alpha \frac{r}{R}\right) \tag{2}$$

where v is the tangential velocity, r is the radial location, ω_c is the angular speed of the engine, R is the cylinder radius,

TABLE 1 Operating conditions

Engine specifications	Measurement
Bore × stroke (mm)	82 × 90.4
Displacement (cm^3)	477.2
Compression ratio	16.4
Squish height at TDC (mm)	0.88
Operating conditions	
Intake pressure (bar)	1.5
Intake temperature (K)	372.15
Engine speed (rpm)	1500
Swirl ratio	1.5,2.2, 3.5

FIGURE 1 Bowl shapes, (a) san_bowl, (b) erl_bowl, (c) cyl_bowl

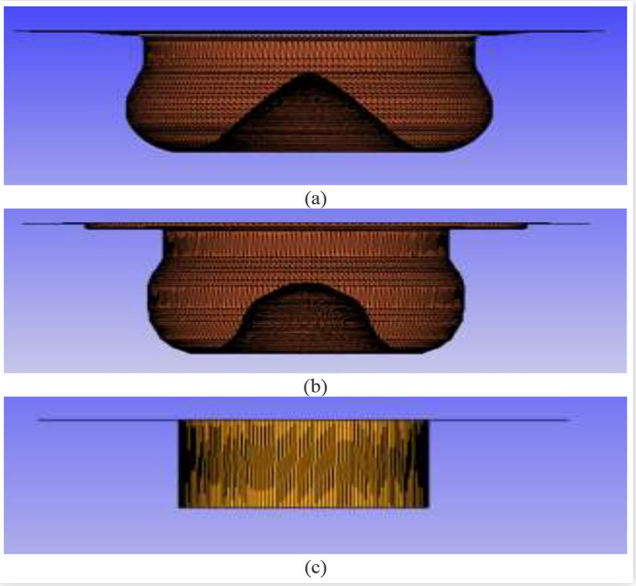

TABLE 2 Important boundary and initial conditions

Physical Parameters	Set-value	
Piston surface temperature (K)	450	
Liner surface temperature (K)	400	
Head surface temperature (K)	400	
Gas composition (mole fraction)	CO_2	0.09
	N_2	0.81
	O_2	0.1

R_{S0} is the steady swirl ratio, and J_1 and J_2 are the first-order and second-order Bessel functions of the first kind, respectively

Bessel function shape parameter, alpha (α) = 2.2 was set as per the recommendation for the modeled engine [30]. A base grid size of 3 mm was used for the computational domain. Adaptive mesh refinement with velocity embedding level = 3 was adopted to resolve the gradients in velocity field. The pressure velocity coupling was solved using the Pressure implicit splitting of operator (PISO) loops. Other important boundary and initial conditions are given in Table 2.

Results and Discussion

Model Validation

The in-cylinder pressure traces from the experiment and CFD during motoring are shown in figure 2. The figure shows that the predicted profile matches satisfactorily with the experimental data. The maximum error observed at TDC was ~2.4%. The objective of this work was to study the in-cylinder flow behavior. The flow structures were not affected by the differences in the thermodynamic properties in this range.

FIGURE 2 In-cylinder pressure variations

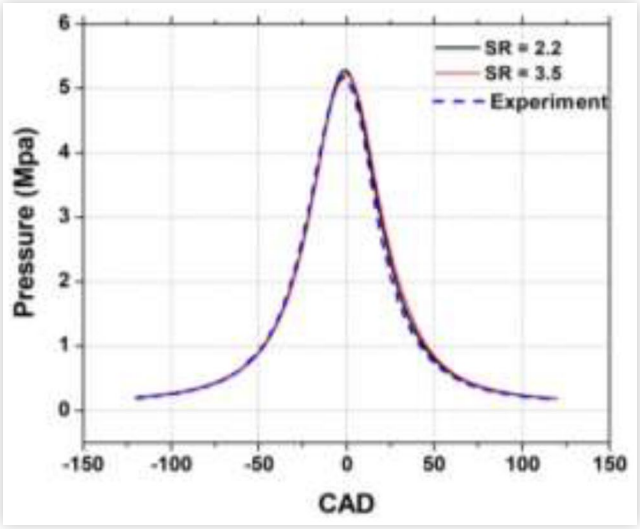

Velocity contours and vector fields (experiment and CFD) are shown in tables 3-6. Same scale was used for all the contours to facilitate quantitative comparison.

The first column shows the velocity magnitude, and the second column shows the flow-field. Experimental results are shown in the first row. The white annular region visible in the experimental velocity contour was due to the image processing

TABLE 3 Velocity magnitude distribution (left column) and flow field (right column)

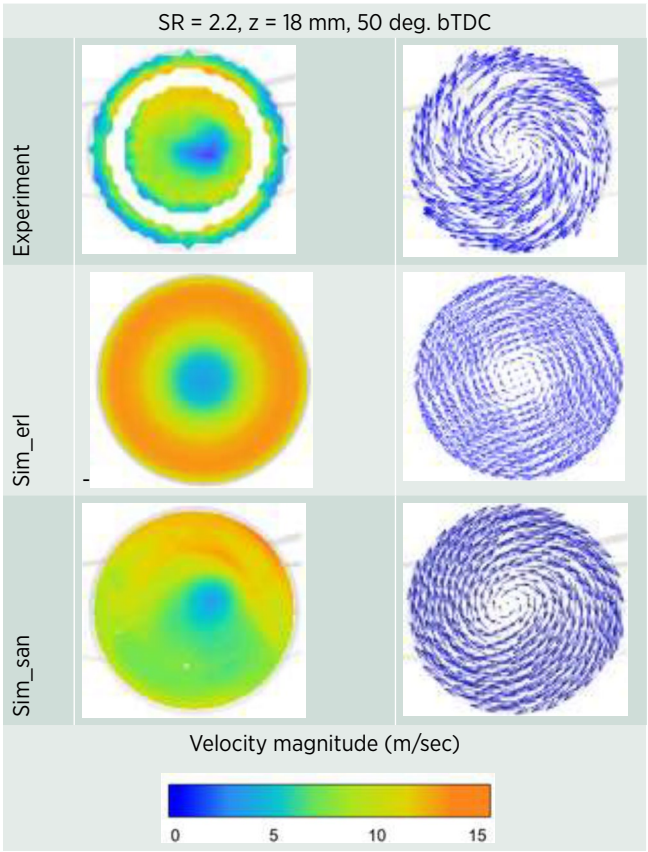

TABLE 4 Velocity magnitude distribution (left column) and flow field (right column)

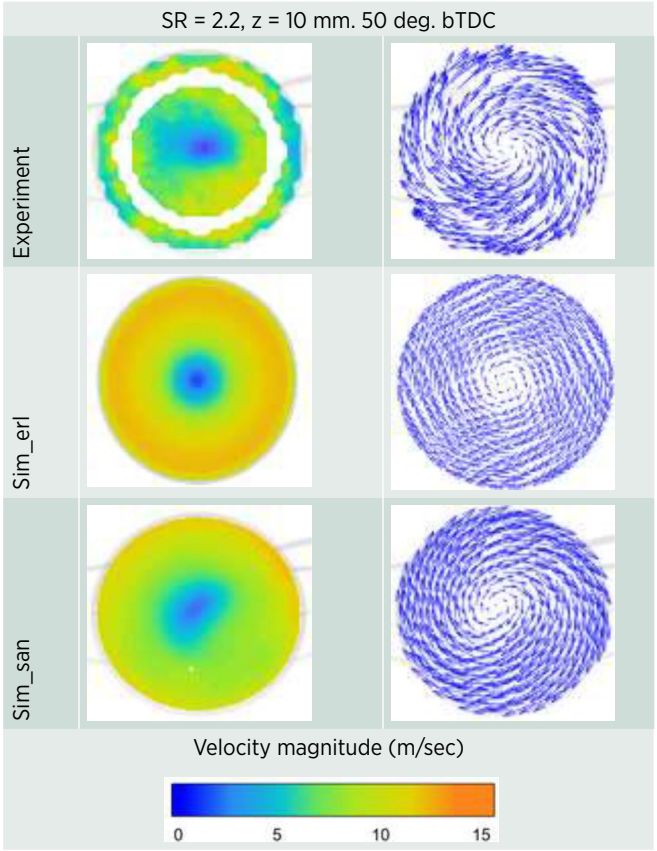

TABLE 5 Velocity magnitude distribution (left column) and flow field (right column)

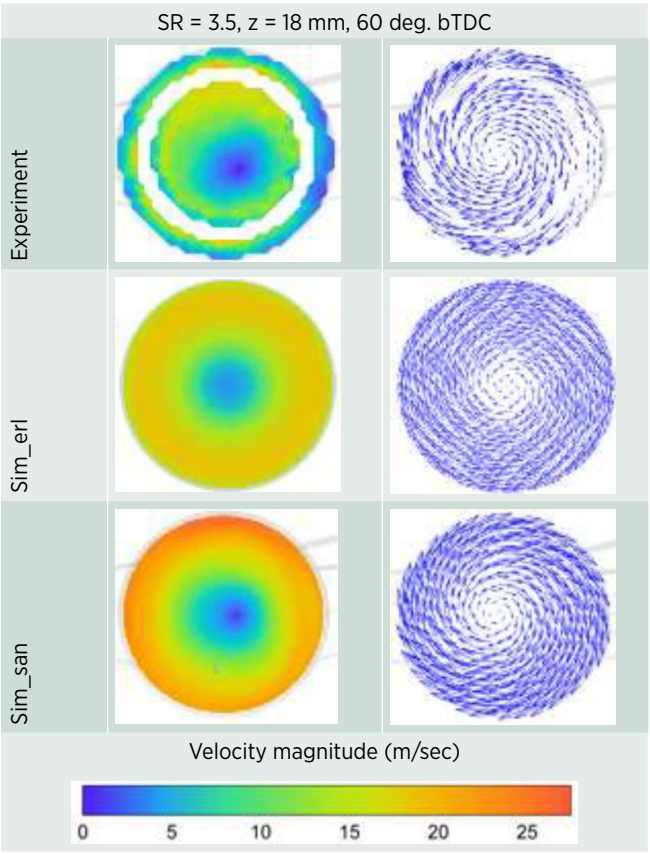

TABLE 6 Velocity magnitude distribution (left column) and flow field (right column)

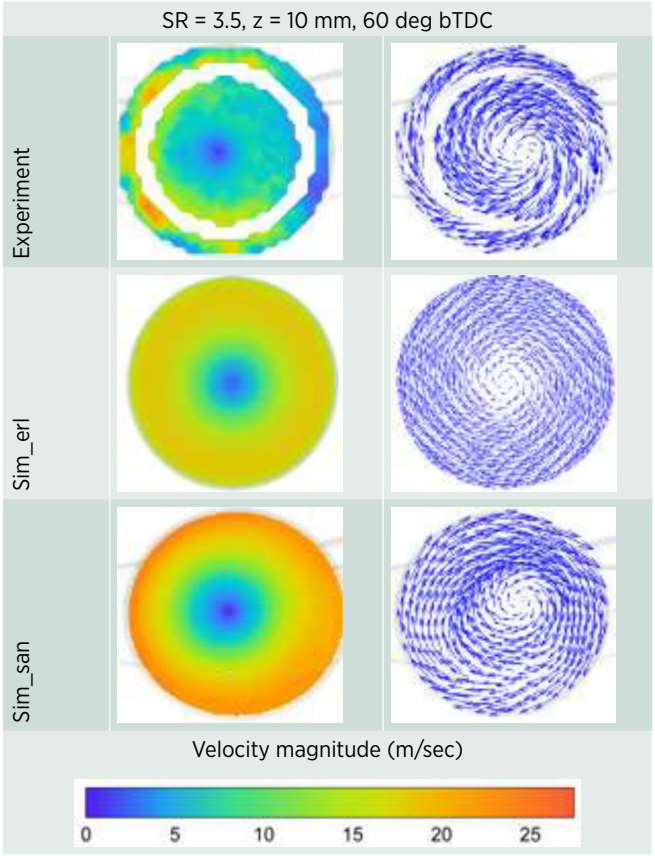

issues near the bowl lip region. CFD predictions of the current work and Sandia National Laboratory are shown in second and third rows, respectively. The data were obtained for two different swirl ratios (2.2 and 3.5) at a distance of z = 10 mm and 18 mm from the fire-deck. The results for SR= 2.2 were obtained at 50° bTDC. For SR=3.5, the crank position was 60° bTDC. As can be seen from figures (Table 3-6), the velocity magnitude distribution was qualitatively similar to the experimental results. The changes in the velocity gradients were captured satisfactorily. However, the sector geometry (Sim_san) was able to capture the asymmetry in velocity distribution for SR_{steady}2.2 case at z = 18 mm. More symmetric distribution can be observed for higher swirl level (SR_{steady} = 3.5) for experiments and simulations. Sim_san slightly over-predicted the velocity near the cylinder wall region compared to sim_erl. The velocity field for all these cases (experiment and CFD) suggested that the flow in the r-ɵ plane was dominated by swirl motion. The small-scale vortices that resulted during the suction were dissipated by the mid-compression stroke, and bulk of energy was carried by the large swirl vortices of the order of cylinder bore.

The variation in instantaneous global swirl ratio with CAD is shown in figure 4 for bowls of different geometry and SR_{steady} = 2.2 case. It could be observed that the SR is almost similar for all the geometries up to -50°aTDC. For the most part of the compression stroke, the flow moves upward with the piston and there is minimal effect of the bowl geometry on the mean flow. The change in SR takes place only after the squish flow starts to be dominant. This usually happens

FIGURE 4 Variation of global swirl-ratio

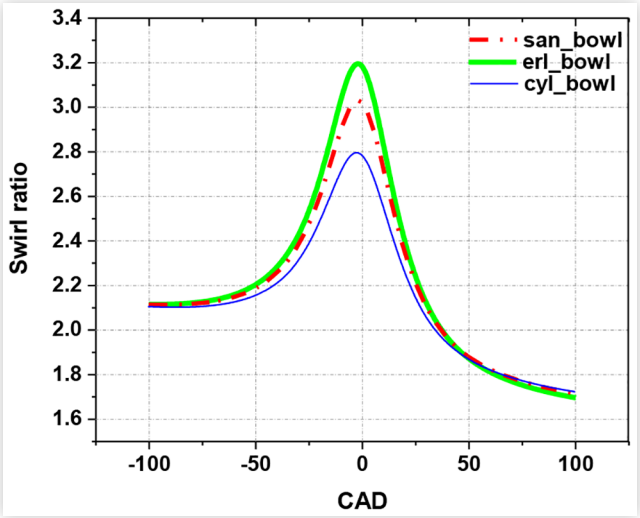

around -40°aTDC. A similar observation was also reported in other studies [31]. Due to conservation of angular momentum, as the fluid element from the squish zone enters the bowl, its tangential velocity increases, thus increasing the swirl. Therefore, increase in swirl near the late compression was governed by the strength of squish and decay rate of angular momentum. The erl_bowl attained higher SR compared to san_bowl because of smaller bowl entry radius, which resulted in higher squish velocity. The cyl_bowl attained minimum SR because it has more homogenous mass distribution thorough out the bowl region. The re-entrant type bowls have higher mass accumulated towards the bowl periphery due to piston-pip. The tangential velocity was higher towards bowl periphery, which resulted in higher angular momentum and SR. A similar trend was observed for SR_{steady} = 3.5 (not shown), as the transfer of radial momentum transferred to the fluid element in the squish zone was independent of swirl. However, the centrifugal forces on the incoming fluid element vary quadratically with SR which play a key role in forming vertical plane structures in the piston bowl near TDC [1].

Table 7 shows the in-cylinder flow structures for two SR_{steady}= 2.2 and 3.5 in three different piston bowls at TDC. These structures contribute to superior fuel-air mixing by generating additional turbulence.

With increasing swirl ratio, velocity magnitude increases because of increased in-cylinder motion of fluid parcels as inferred from the following equation:

$$\text{Swirl ratio} = \frac{\omega_s}{2\pi N} \tag{3}$$

where ω_s is the angular velocity of a solid-body rotating flow, which has equal angular momentum to the actual flow.

As shown in the figure, dual vortex formation was observed for all piston profiles. However, in SR_{steady}2.2, the magnitude of formation of counter-clockwise vortex structure was not as strong as in SR_{steady} 3.5. Similar flow-structures were also reported in other studies [32, 33]. Transport and deflection of high momentum fluid by the piston bowl geometry was the primary reason for the formation of

TABLE 7 Vertical plane flow structures inside piston bowl at TDC for different geometries

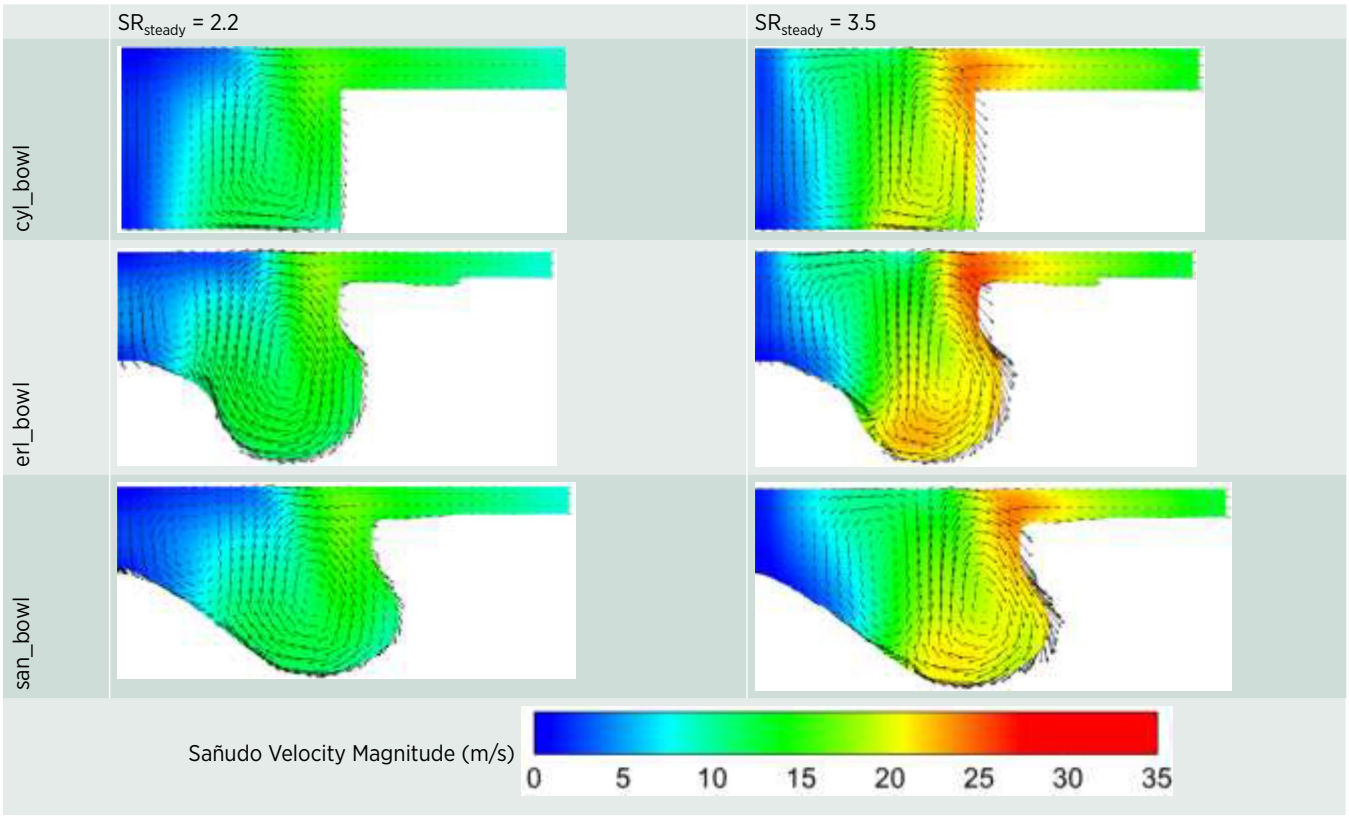

observed vortices. As the piston approaches TDC, squish flow starts increasing. These fluid parcels in the squish area are pushed towards the bowl center. However, the centrifugal force of the swirling fluid restricts the radial penetration. Therefore, the squish flow bends into the piston bowl. As the piston reaches TDC, high momentum fluid strikes the bottom of the bowl and gets deflected upwards. By virtue of this, the fluid parcels start moving upward and try to re-enter the bowl. However, due to centrifugal forces, these parcels are pushed towards the bowl periphery. Thus, a vortex gets formed near the bowl periphery. A counter-rotating vortex also develops near the bowl center. Careful observation in geometries of san_bowl and erl_bowl revealed that the piston pip gradient was almost constant for the former, wherein the latter bowl had a steep change in the gradient. The steeper gradient in erl_bowl deflected the fluid earlier than the san_bowl. Thus, re-entry in the case of erl_bowl was closer to the bowl periphery compared to san_bowl. Flow structures were similar for the SR_{steady} 3.5 case. The velocity magnitude, in this case, was higher compared to SR = 2.2 case due to higher angular momentum. It was observed that the clockwise vortex was pushed more towards the bowl periphery for all three geometries. As a result, the interface between the two counter-rotating vortices shifted. The formation of vortices and the piston pip geometry affected the rigid body motion of swirl vortices. The squish generated flow structures have a significant contribution in turbulence generation [34]. The turbulence generation is given by the following equation:

$$P_{r\theta} = -\left\langle u_r' u_\theta' \right\rangle \left(\frac{1}{r} \frac{\partial \langle U_r \rangle}{\partial \theta} + \frac{\partial \langle U_\theta \rangle}{\partial r} - \frac{\langle U_\theta \rangle}{r} \right) \tag{4}$$

The first term in the bracket is the contributed by the asymmetry of radial velocity in the r-θ plane. The difference in the second and third term represents deviation of the flow-field from the rigid body motion. Therefore, the gradient in tangential velocity plays a major role in turbulence generation. In the subsequent sections, this aspect was analyzed.

Figure 5 (a-d) shows the variation of radial and tangential velocity profiles with distance from the bowl center for different geometries under consideration. The radius (r) has been normalized by bowl entry radius (R) for each geometry to facilitate comparison. The normalized radius is given by r* = r/R. The in-plane velocity was assumed positive for vertically upward and horizontally rightward direction (from center towards periphery). It was observed (figure 5 a) that the radial velocity changed sign for all three cases as we move from the center towards the periphery. This was attributed to the presence of two counter-rotating vortices inside the bowl. The sign change occurs near the interface of the two vortices. The vortex near the center has an anticlockwise sense. Therefore, moving from the center to the periphery, the radial component of velocity is negative. The magnitude of radial velocity decreases as we move towards the edge of the vortex. The field becomes more vertical due to its curvature (as observed from Table 7). Finally, it changes sign through the interface of the two vortices. The radial velocity again starts increasing with the radius as we move into the vortex near the periphery. This vortex is clockwise. A similar trend was observed for other two bowl geometries. Previous studies reported that the re-entrant bowl and cylindrical bowl have similar flow structures near the TDC [1]. However, it can be observed that the erl_bowl and san_bowl have higher radial velocity near the periphery compared to the cylindrical bowl. Smaller squish height was the reason behind this. Figure 5(b) shows the variation of tangential velocity with a normalized radius. It was observed that the velocity profile for cyl_bowl was closer to a rigid body like motion. The other two geometries showed significant deviations from rigid-body motion. A sudden change in gradient in velocity profile occurred right after the radial velocity changed sign (figure 5a). This may have been due to the re-entry of squish flow after deflecting from the bowl, which resulted in clockwise vortex. Additional momentum added could be the reason for increased tangential velocity. The profile varied almost linearly, up to the periphery. Velocity decreased at the periphery, possibly due to the wall boundary effect.

Figures 5 (c-d) showed the variation of radial and tangential velocity for higher swirl ratios (SR_{steady} = 3.5). From figure 5(c), it can be observed that the radial velocity changed sign at a higher radius compared to SR_{steady} = 2.2 case. The trend was similar for all bowl geometries investigated. This confirmed the shifting of vortices at a higher swirl ratio, as discussed earlier. Therefore, the re-entry of the squish flow occurred relatively closer to the periphery. This resulted in higher mass accumulation and hence higher angular momentum. From figure 5(d), the effect of vortex center shifting can be observed. Change in velocity gradient occurs farther away from the bowl center compared to low swirl case. These observations were in agreement with the flow structures observed in the figure (Table 7).

The radial variations of TKE are shown in figure 6(a-b). Higher TKE was observed for SR_{steady} =3.5 case for all geometries. For SR_{steady} = 2.2 case, maximum TKE was attained near normalized radius (r*) = 0.4, which was also the location of interface of the two vortices (radial velocity changes sign, as discussed for figure 6a). For SR_{steady} = 3.5 case, the maxima for TKE was attained between r* = 0.4 and 0.6 for all three geometries. This coincided with the sudden change in the velocity gradient of tangential velocity for the same SR_{staedy} (figure 5d). Therefore, the deviation of the swirl structure from rigid body rotation had a significant effect on the TKE. This could be attributed to turbulence generation, as given by the equation. The maximum TKE values for cyl_bowl and san_bowl were similar. However, the maxima of san_bowl was slightly shifted compared to cyl_bowl. This could be explained with the help of radial velocity distribution (figure 5c). As discussed earlier, the sign change of radial velocity occurred near the vortices interface. From figure 5(c), it can be observed that this location was closer to the bowl center for cyl_bowl compared to the san_bowl. This could be the reason behind the location of maxima of cyl_bowl. The erl_bowl resulted in the maximum TKE for both swirl ratios investigated. The cyl_bowl attained higher TKE compared to the san_bowl near the bowl center for higher swirl case. Due to increased centrifugal forces at higher swirl level, the fluid mass is pushed outward. In case of san_bowl, due to the presence of piston pip, higher fraction of mass tends to accumulate towards periphery. However, in case of cyl_bowl, the mass is more evenly distributed. Also, the boundary layer effect of the piston pip could have decreased the velocity near the bowl

FIGURE 5 Variation of radial and tangential velocity with radius

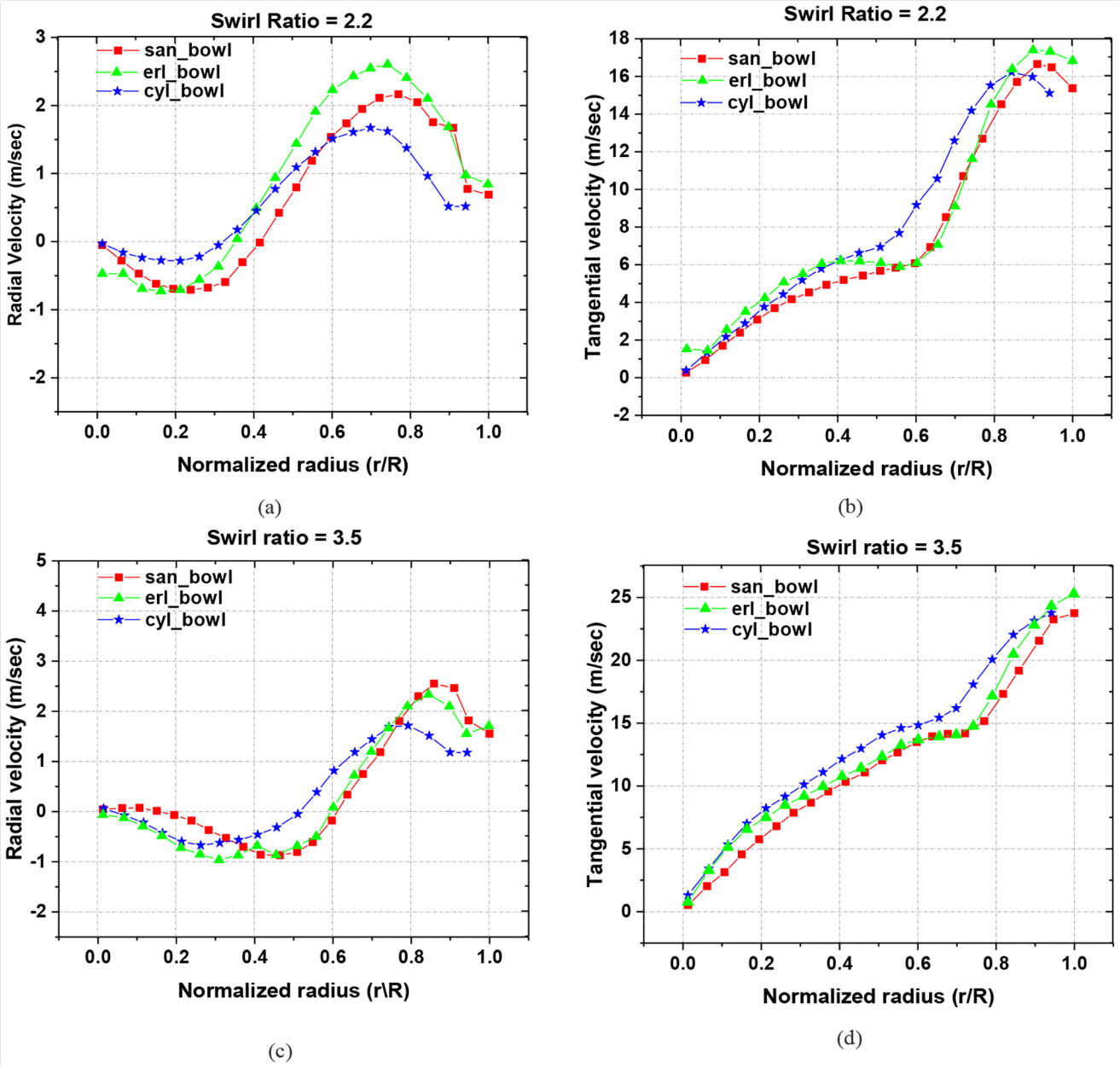

center for the former. This is also evident from radial and tangential velocity distribution (Figure 5 c-d). Higher velocity of re-entry resulted from steep piston pip gradient and deep bowl geometry, that ensured higher value of TKE for the erl_bowl.

Figures 7(a-b) showed the variations of mean TKE values for all cases investigated. During the late compression stroke, mean TKE values decreased as the piston moved closer to the TDC for san_bowl and cyl_bowl. However, for erl_bowl, the magnitude increased first and then decreased. Similar trends were observed for both swirl ratios. This was attributed to the competing effects of the decay rate of angular momentum, turbulence dissipation, and turbulence production. Further exploration of the role of piston pip gradient and bowl-depth was required to gain more insights into these observations.

Conclusions

In this study, sector geometry model was simulated using CONVERGE CFD under motoring conditions. Modeling results were validated using the experimental data obtained from PIV experiments done in a light-duty optical engine. Some of the major observations from the study are as follows: The velocity contour and gradients were qualitatively similar to the experimental results. The results were also compared with the results of full geometry simulation. Full geometry simulation could capture the flow field more accurately then the one in sector case. The maximum and minimum velocity were similar for both cases. However, the flow asymmetry could not be captured by the current approach. This might

FIGURE 6 Variations of TKE with radius

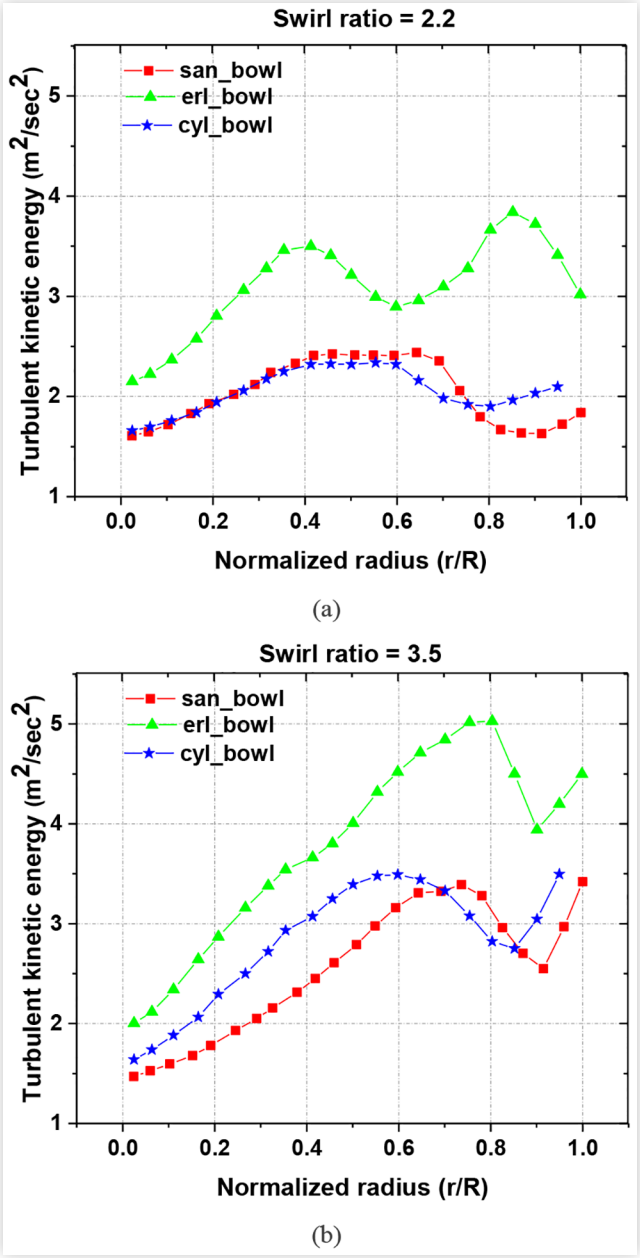

FIGURE 7 Variations of TKE with CAD at (a) SR= 2.2 (b) SR = 3.5

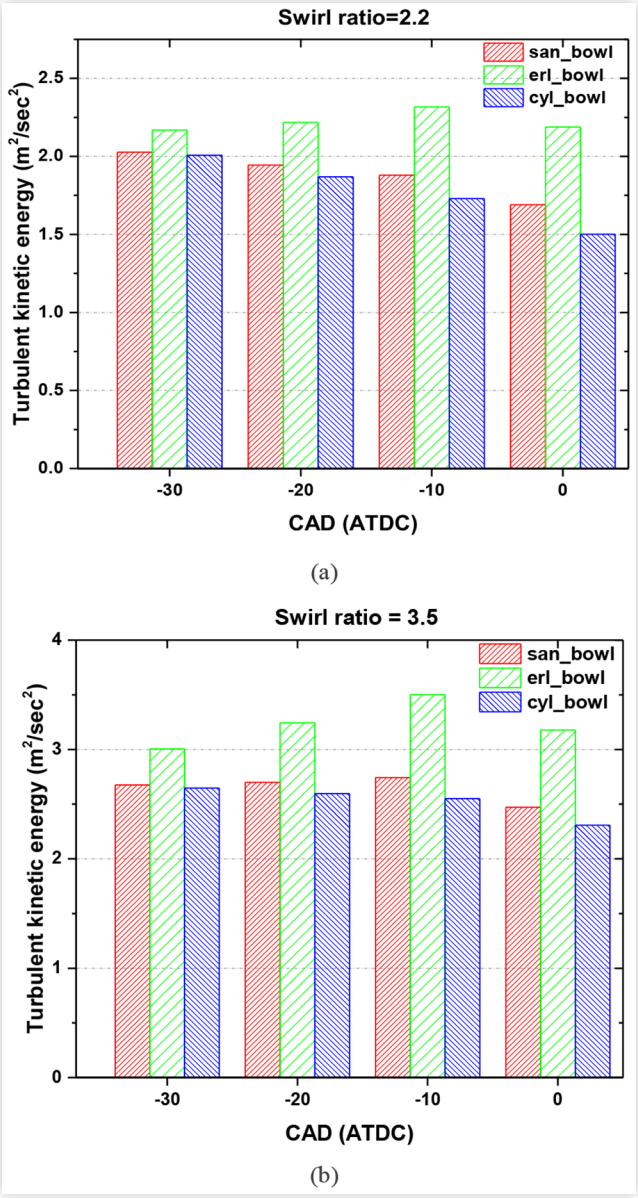

lead to an incorrect prediction of emissions for partially premixed combustion, where mixture stratification plays a key role. Late compression flow structures were similar to the ones reported by other studies. Thus, the approach may be suitable for a qualitative comparison of different geometries and optimization studies having relatively lower computational time. Minimum velocity of the same order was observed near the central region of the piston bowls. Hence initial spray development may not be affected by the bowl geometry. Discrete point data obtained from the swirl plane were related to the flow-structures inside the piston bowl. This could be of great importance to those optical engines, which don't do not have access to the combustion chamber during late compression (near TDC), which is crucial for fuel-air mixing and combustion. Locations of these vortices formed were responsible for the distribution of TKE in the combustion chamber. Vortex orientation can be altered by changing the swirl levels in the engine. The erl_bowl attained the maximum TKE values for both swirl ratios investigated. Strong squish flow was observed at lower swirl ratio. Higher value of TKE was observed for cyl_bowl near the bowl center, despite having lower global swirl ratio compared to san-bowl. Thus, global swirl ratio may not be a deciding parameter for prediction of in-cylinder turbulence during late compression. The piston pip shape and gradient also have a significant effect on the bowl vortices and TKE. Therefore, swirl ratio and piston geometry should be optimized together to achieve superior results. Further investigations on the effect of swirl level and spray swirl interactions could help in developing swirl control strategies for optimization of the engine performance for emission compliance in future.

References

1. Miles, P.C., "Turbulent Flow Structure in Direct-Injection, Swirl-Supported Diesel Engines," . In: *Flow and Combustion in Reciprocating Engines*. (Springer, Berlin, Heidelberg, 2008), 173-256.
2. Liou, T. and Santavicca, D., "Cycle Resolved Turbulence Measurements in a Ported Engine with and without Swirl," SAE Technical Paper 830419, 1983. https://doi.org/10.4271/830419.
3. Liou, T.-M., Hall, M., Santavicca, D.A., and Bracco, F.V., "Laser Doppler Velocimetry Measurements in Valved and Ported Engines," SAE Technical Paper 840375, 1984. https://doi.org/10.4271/840375.
4. Bopp, S., Vafidis, C. and Whitelaw, J.H., "The Effect of Engine Speed on the TDC Flow Field in a Motored Reciprocating Engine," SAE Technical Paper 860023, 1986, https://doi.org/10.4271/860023.
5. Dimopoulos, P. and Boulouchos, K., "Turbulent Flow Field Characteristics in a Motored Reciprocating Engine," SAE Technical Paper 972833, 1997. https://doi.org/10.4271/972833.
6. Ikegami, M., Shioji, M., and Nishimoto, K., "Turbulence Intensity and Spatial Integral Scale during Compression and Expansion Strokes in a Four-Cycle Reciprocating Engine," SAE Technical Paper 870372, 1987. https://doi.org/10.4271/870372.
7. Hall, M.J. and Bracco, F.V., "A Study of Velocities and Turbulence Intensities Measured in Firing and Motored Engines," SAE Technical Paper 870453, 1987. https://doi.org/10.4271/870453.
8. Heim, D. and Ghandhi, J., "A Detailed Study of In-Cylinder Flow and Turbulence Using PIV," *SAE International Journal of Engines* 4(1):1642-1668, 2011. https://doi.org/10.4271/2011-01-1287.
9. Gafoor, C.P.A. and Gupta, R., "Numerical Investigation of Piston Bowl Geometry and Swirl Ratio on Emission from Diesel Engines," *Energy Conversion and Management* 101:541-551, 2015.
10. Gosman, A.D., "Flow Processes in Cylinders," In: Horlock, J.H. and Winterbone, D.E., The Thermodynamics and Gas Dynamics of Internal-Combustion Engines. Volume II, 1986.
11. Bopp, S., Vafidis, C., and Whitelaw, J.H., "The Effect of Engine Speed on the TDC Flow Field in a Motored Reciprocating Engine," SAE Technical Paper 860023, 1986. https://doi.org/10.4271/860023.
12. Vafidis, C., "Influence of Induction Swirl and Piston Configuration on Air Flow in a Four-Stroke Model Engine," *Proceedings of the Institution of Mechanical Engineers, Part C: Journal of Mechanical Engineering Science* 198(2):71-79, 1984.
13. Eismark, J., Balthasar, M., Karlsson, A., Benham, T. et al., "Role of Late Soot Oxidation for Low Emission Combustion in a Diffusion-Controlled, High-EGR, Heavy Duty Diesel Engine," SAE Technical Paper 2009-01-2813, 2009. https://doi.org/10.4271/2009-01-2813.
14. Eismark, J., Andersson, M., Christensen, M., Karlsson, A., and Denbratt, I., "Role of Piston Bowl Shape to Enhance Late-Cycle Soot Oxidation in Low-Swirl Diesel Combustion," *SAE International Journal of Engines* 12(3):233-250, 2019. https://doi.org/10.4271/03-12-03-0017.
15. Belgiorno, G., Boscolo, A., Dileo, G., Numidi, F. et al., "Experimental Study of Additive-Manufacturing-Enabled Innovative Diesel Combustion Bowl Features for Achieving Ultra-Low Emissions and High Efficiency," *SAE Int. J. Adv. & Curr. Prac. in Mobility* 3(1):672-684, 2021. https://doi.org/10.4271/2020-37-0003.
16. Li, X., Chen, Y., Liwang, S., and Liu, F., "Effects of Lateral Swirl Combustion Chamber Geometries on the Combustion and Emission Characteristics of DI Diesel Engines and a Matching Method for the Combustion Chamber Geometry," *Fuel* 224:644-660, 2018.
17. Xu, L., Bai, X.S., Li, Y., Treacy, M. et al., "Effect of Piston Bowl Geometry and Compression Ratio on In-Cylinder Combustion and Engine Performance in a Gasoline Direct-Injection Compression Ignition Engine under Different Injection Conditions," *Applied Energy* 280:115920, 2020.
18. Benajes, J., Pastor, J.V., García, A., and Monsalve-Serrano, J., "An Experimental Investigation on the Influence of Piston Bowl Geometry on RCCI Performance and Emissions in a Heavy-Duty Engine," *Energy Conversion and Management* 103:1019-1030, 2015.
19. Zha, K., Busch, S., Miles, P.C., Wijeyakulasuriya, S. et al., "Characterization of Flow Asymmetry during the Compression Stroke using Swirl-Plane PIV in a Light-Duty Optical Diesel Engine with the Re-Entrant Piston Bowl Geometry," *SAE International Journal of Engines* 8(4):1837-1855, 2015. https://doi.org/ 10.4271/2015-01-1699.
20. Fridriksson, H.S., Tuner, M., Andersson, O., Sunden, B. et al., "Effect of Piston Bowl Shape and Swirl Ratio on Engine Heat Transfer in a Light-Duty Diesel Engine," SAE Technical Paper 2014-01-1141, 2014. https://doi.org/10.4271/2014-01-1141.
21. Deslandes, W., Dumont, P., Dupont, A., Baby, X. et al., "Airflow Cyclic Variations Analysis in Diesel Combustion Chamber by PIV Measurements," SAE Technical Paper 2004-01-1410, 2004. https://doi.org/10.4271/2004-01-1410.
22. Achuth, M. and Mehta, P.S., "Predictions of Tumble and Turbulence in Four-Valve Pentroof Spark Ignition Engines," *International Journal of Engine Research* 2(3):209-227, 2001.
23. Tahry, S.H.E.I., "A Numerical Study on the Effects of Fluid Motion at Inlet-Valve Closure on Subsequent Fluid Motion in a Motored Engine," SAE Technical Paper 820035, 1982. https://doi.org/10.4271/820035.
24. Huang, M., Gowdagiri, S., Cesari, X.M., and Oehlschlaeger, M.A., "Diesel Engine CFD Simulations: Influence of Fuel Variability on Ignition Delay," *Fuel* 181:170-177, 2016.
25. Kodavasal, J., Kolodziej, C.P., Ciatti, S.A., and Som, S., "Effects of Injection Parameters, Boost, and Swirl Ratio on Gasoline Compression Ignition Operation at Idle and Low-Load Conditions," *International Journal of Engine Research* 18(8):824-836, 2017.
26. Zou, X., Hu, W., Zheng, Z., Reitz, R., and Yao, M., "Numerical Study of the RCCI Combustion Processes Fuelled with Methanol, Ethanol, n-Butanol and Diesel," SAE Technical Paper 2016-01-0777, 2016. https://doi.org/10.4271/2016-01-0777.

27. Perini, F., Zha, K., Busch, S., Miles, P.C. and Reitz, R.D., "Principal Component Analysis and Study of Port-Induced Swirl Structures in a Light-Duty Optical Diesel Engine," No. SAND2015-1632C, Sandia National Lab. (SNL-NM), Albuquerque, NM, 2015.
28. Senecal, P.K., Richards, K.J., Pomraning, E., Yang, T. et al., "A New Parallel Cut-Cell Cartesian CFD Code for Rapid Grid Generation Applied to In-Cylinder Diesel Engine Simulations," SAE Technical Paper 2007-01-0159, 2007. https://doi.org/10.4271/2007-01-0159.
29. Johnston, S.C., Robinson, C.W., Smith, R.W., Smith, J.R., and Witze, P.O., "Application of Laser Diagnostics to an Injected Engine," SAE Technical Paper 790092, 1979. https://doi.org/10.4271/790092.
30. Perini, F., Dempsey, A., Reitz, R.D., Sahoo, D. et al., "A Computational Investigation of the Effects of Swirl Ratio and Injection Pressure on Mixture Preparation and Wall Heat Transfer in a Light-Duty Diesel Engine," SAE Technical Paper 2013-01-1105, 2013. https://doi.org/10.4271/2013-01-1105.
31. Perini, F., Zha, K., Busch, S., Kurtz, E. et al., "Piston Geometry Effects in a Light-Duty, Swirl-Supported Diesel Engine: Flow Structure Characterization," *International Journal of Engine Research* 19(10):1079-1098, 2018.
32. Arcoumanis, C., Bicen, A.F., and Whitelaw, J.H., "Squish and Swirl-Squish Interaction in Motored Model Engines," *J. Fluids Eng.* 105(1):105-112, 1983.
33. Lin, L., Shulin, D., Jin, X., Jinxiang, W., and Xiaohong, G., "Effects of Combustion Chamber Geometry on In-Cylinder Air Motion and Performance in DI Diesel Engine," SAE Technical Paper 2000-01-0510, 2000. https://doi.org/10.4271/2000-01-0510.
34. Zhang Shurui, S.S.L.S., "A Study of the Energy Conversion of the Gas Flow and the Variation of the Turbulent Flow Field in the Cylinder during Compression Stroke of a DI Diesel Engine," *Transactions of CSICE* 1, 1990.

Acknowledgements

Authors gratefully acknowledge the Engine Combustion Network (ECN) and its collaborators for making the experimental data available for modeling, simulation and validation.

Abbreviation

BTDC - Before top dead center

ATDC - After top dead center

SR - Global swirl ratio (instantaneous)

TKE - Turbulent kinetic energy

CA - Crank angle

ISSN 0148-7191